


Article

Magnetic Properties and Magnetocaloric Effect in $\text{Gd}_{100-x}\text{Co}_x$ Thin Films

Mohamed Tadout ^{1,2}, Charles-Henri Lambert ^{3,4}, Mohammed Salah El Hadri ^{3,5} , Abdelilah Benyoussef ^{1,2}, Mohammed Hamedoun ², Mohammed Benaissa ¹, Omar Mounkachi ^{1,*} and Stéphane Mangin ³

¹ Laboratoire de Matière Condensée et Sciences Interdisciplinaires (LaMCScI), B.P. 1014, Faculty of Science-Mohammed V University, 11000 Rabat, Morocco; tadout.mohamed@um5s.net.ma (M.T.); a.benyoussef@mascir.com (A.B.); benaissa@fsr.ac.ma (M.B.)

² Materials and Nanomaterials Centre, Moroccan Foundation for Advanced Science, Innovation and Research, MAScIR, 11000 Rabat, Morocco; m.hamedoun@mascir.com

³ Institut Jean Lamour, UMR CNRS 7198, Université de Lorraine, 54000 Nancy, France; charles-henri.lambert@mat.ethz.ch (C.-H.L.); melhadri@ucsd.edu (M.S.E.H.); stephane.mangin@univ-lorraine.fr (S.M.)

⁴ Laboratory for Magnetism and Interface Physics, Department of Materials, ETH Zurich, 8093 Zurich, Switzerland

⁵ Center for Memory and Recording Research, University of California San Diego, La Jolla, CA 92093-0401, USA

* Correspondence: o.mounkachi@gmail.com

Received: 22 March 2019; Accepted: 16 May 2019; Published: 28 May 2019



Abstract: We investigated the magnetic and magnetocaloric properties of $\text{Gd}_{100-x}\text{Co}_x$ ($x = 40$ to 56) thin films fabricated by the sputtering technique. Under an applied field change $\Delta H = 20$ kOe, the magnetic entropy change (ΔS_m) decreases from $2.64 \text{ Jkg}^{-1}\text{K}^{-1}$ for $x = 44$ to about $1.27 \text{ Jkg}^{-1}\text{K}^{-1}$ for $x = 56$. Increasing the Co concentration from $x = 40$ to 56 shifts the Curie temperature of $\text{Gd}_{100-x}\text{Co}_x$ ($x = 40$ to 56) thin films from 180 K toward 337 K. Moreover, we extracted the values of critical parameters T_c , β , γ , and δ by using the modified Arrott plot methods. The results indicate the presence of a long-range ferromagnetic order. More importantly, we showed that the relative cooling power (RCP), which is a key parameter in magnetic refrigeration applications, is strongly enhanced by changing the Co concentration in the $\text{Gd}_{100-x}\text{Co}_x$ thin films. Our findings help pave the way toward the enhancement of the magnetocaloric effect in magnetic thin films.

Keywords: magnetocaloric effects (MCE); thin films; universal scaling analysis; critical exponents

1. Introduction

The study of the magnetocaloric effect as a means for magnetic cooling has attracted rising interest due to the prospect of replacing conventional refrigeration systems [1,2]. Recently, various experimental and theoretical works have been carried out on magnetic materials showing a large magnetocaloric effect [3,4]. Moreover, many studies of the magnetocaloric effect (MCE) for ambient applications have been performed on rare-earth based compounds, since the latter show high magnetic moments. However, the MCE was found to be rather small for this class of material. Indeed, the largest MCE was reported for the rare-earth element Gd, where the ΔS_M value goes up to $-9.8 \text{ Jkg}^{-1}\text{K}^{-1}$ and ΔT_{ad} near $T_c = 293$ K is about 11.6 K for a magnetic field change of 5T [5]. In 1997, Pecharsky and Gschneidner demonstrated in their pioneering work a giant MCE in the compound $\text{Gd}_5\text{Si}_2\text{Ge}_2$ [6], a discovery that reawakened interest in magnetic refrigeration for ambient applications. Later, several different classes of materials were found to exhibit giant MCEs near room temperature, such as $\text{MnAs}_{1-x}\text{Sb}_x$ [7],

La(Fe_{1-x}Si_x)₁₃ [8] and their hydrides [9], MnFeP_{1-x}As_x [10], as well as Ni_{0.5}Mn_{0.5-x}Sn_x [11]. However, most these investigations were limited to the investigation of the MCE in bulk materials, while works on magnetic thin films are very limited.

Recently, the study of the MCE in thin films has triggered more interest, namely the study of Gd/W multilayers [12,13], manganites [14,15], FeRh [16], NiMnGa [17], and MnAs [18]. From a technological point of view, the use of magnetic refrigerant in the form of thin films, powders, or wires is more desirable [5,19–21]. In this context, many magnetic coolers based on Gd powders and laminate structures were demonstrated [1]. More recently, many studies have investigated the effect of the dimensionality reduction on MCE parameters [13,22–24]. Indeed, it was recently reported that the reduction of dimensionality in a ferromagnetic material broadens the paramagnetic to ferromagnetic (PM-FM) transition, shifts it to lower temperatures, and also reduces the magnetization saturation and magnitude of (ΔS_m) [22]. On the other hand, the broadening of (ΔS_m) in thin films should enhance the relative cooling power (RCP), which is preferable for magnetic refrigeration. In this work, we have investigated the impact of the substitution of gadolinium with cobalt in thin film form on the magnetic and magnetocaloric properties of Gd_{100-x}Co_x alloys. We have developed and optimized the magnetic properties of Gd_{100-x}Co_x thin film alloys deposited by sputtering techniques, and then derived temperature dependence of the entropy change [25].

2. Experimental Method

The thin films were deposited at room temperature on (100)-silicon substrates by the sputtering deposition technique. The chamber base pressure was 10⁻⁷ Torr. A 3 nm-thick Ta layer was used as a buffer layer, while a 3 nm-thick Ta capping layer was used to prevent the oxidation of the rare-earth elements. The deposition rates for Gd and Co targets at 50 W and 100 W were 0.719 Å/s and 0.456 Å/s, respectively. The thickness of Gd_{100-x}Co_x (40 < x < 56) alloy films was kept constant and equal to 100 nm in order to ease the comparison of the magnetocaloric values. The Gd_{100-x}Co_x (40 < x < 56) alloy films mostly consisted of an amorphous phase, as depicted in the measured XRD patterns (see Supplementary Materials, Figure S1 for XRD patterns of the studied Gd-Co alloy thin films). The magnetic characterization was carried out using a Quantum Design© SQUID-VSM, where the magnetic field is applied in the sample plane.

3. Results and Discussion

3.1. Magnetic Properties

We measured the temperature dependence of magnetization for all the studied alloy films to determine the temperature as well as the nature of the transition. Figure 1a shows the temperature dependence of the magnetization obtained under an applied magnetic field of 500 Oe for Gd_{100-x}Co_x alloy films with different Co concentrations x = 56, 52, 48, 44, and 40. The PM-FM transition temperature T_c shown in the inset corresponds to the minimum of dM/dT. The obtained values for T_c are 190 K for Gd₆₀Co₄₀, 205 K for Gd₅₆Co₄₄, 240 K for Gd₅₂Co₄₈, 282 K for Gd₄₈Co₅₂, and 335 K for Gd₄₄Co₅₆, respectively. It can be clearly seen from Figure 1b that the T_c of the studied Gd_{100-x}Co_x alloy films increases as a function of the Co concentration x, which is mainly due to the strong Co-Co ferromagnetic exchange interaction. Indeed, any nearest neighbor of Co interacts ferromagnetically regardless of the crystal structure [26].

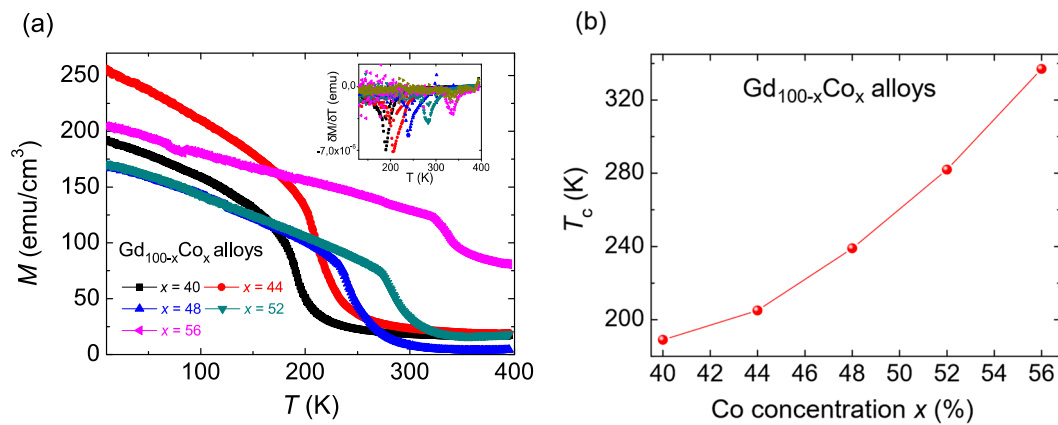


Figure 1. (a) Temperature dependence of magnetization in the studied $Gd_{100-x}Co_x$ alloys for various compositions under an applied field of 500 Oe. The inset shows the derivative curves of dM/dT as a function of T . (b) Evolution of T_c as a function of the Co concentration x .

3.2. Magnetocaloric Effect Properties

Figure 2a shows isothermal magnetization $M(H)$ curves measured for $Gd_{56}Co_{44}$ alloy film under an applied magnetic field up to $\Delta H = 20$ kOe and a temperature ranging from 150 to 290 K. The magnetization curves below the T_c show a non-linear behavior with a tendency towards saturation under the applied magnetic field, which indicates a ferromagnetic behavior. However, the magnetization above the T_c shows a linear behavior, which reflects a paramagnetic behavior. The latter is due to the thermal agitation which disarranges the magnetic moments. In order to determine the nature of the transition in $Gd_{56}Co_{44}$ alloy film, we used the Arrott plot method and employed the Inoue-Shimizu model [27]. According to the Banerjee criteria [28], the positive (resp. negative) slope of the $M^2(H/M)$ curves indicates a second- (resp. first-) order transition. As shown in Figure 2b, only positive slopes of the $M^2(H/M)$ curves were observed for the $Gd_{56}Co_{44}$ alloy film, indicating that the PM-FM transition is a second order transition.

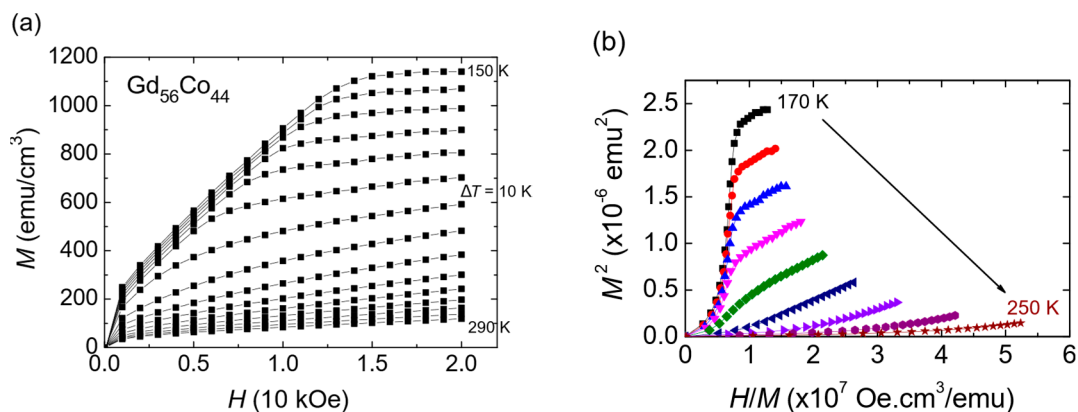


Figure 2. (a) Magnetization isotherms curves and (b) Arrott plots of isotherms in the vicinity of T_c for the $Gd_{56}Co_{44}$ alloy film.

Based on the magnetization curves shown in Figure 2a, the isothermal magnetic entropy change caused by the variation of the applied magnetic field from 0 to $\Delta H = 20$ kOe can be determined by using the Maxwell relation:

$$\Delta S_M(T, H_0) = \mu_0 \sum_i \frac{M_{i+1}(T_{i+1}, H) - M_i(T_i, H)}{T_{i+1} - T_i}$$

We compared the values of $-\Delta S_M$ obtained for the investigated $Gd_{100-x}Co_x$ alloys with $x = 56, 52, 48, 44,$ and 40 with those obtained for a 100 nm-thick Gd layer, as depicted in Figure 3b. The maximum values of the $-\Delta S_M^{\text{peak}}$ (T) curves are obtained close to T_c . The peak temperature in $-\Delta S_M$ (T) is shifted towards high temperature by increasing x , which is most likely due to the enhancement of the Gd–Co indirect interaction. Figure 3b shows the evolution of the peak entropy change value and its full width at half maximum (FWHM) as a function of the Co concentration x . It can be clearly seen that the decrease in peak $-\Delta S_M$ is accompanied by an increase of the FWHM. The maximal entropy change is observed for $x = 44$, and is about 2.65 J/kg.K. Figure 3c shows the evolution of $-\Delta S_M^{\text{peak}}$ as a function of $T_c^{-2/3}$ for the investigated $Gd_{100-x}Co_x$ alloys ($x = 40, 44, 48, 52, 56$) under the applied magnetic field of 2 T. It can be seen from Figure 3b that $-\Delta S_M^{\text{peak}}$ changes linearly with $T_c^{-2/3}$ (or $(708.8-8.83x)^{-2/3}$ with a linear correlation coefficient above 0.992), indicating that $-\Delta S_M^{\text{peak}}$ of the $Gd_{100-x}Co_x$ alloys can be easily tailored by adjusting x .

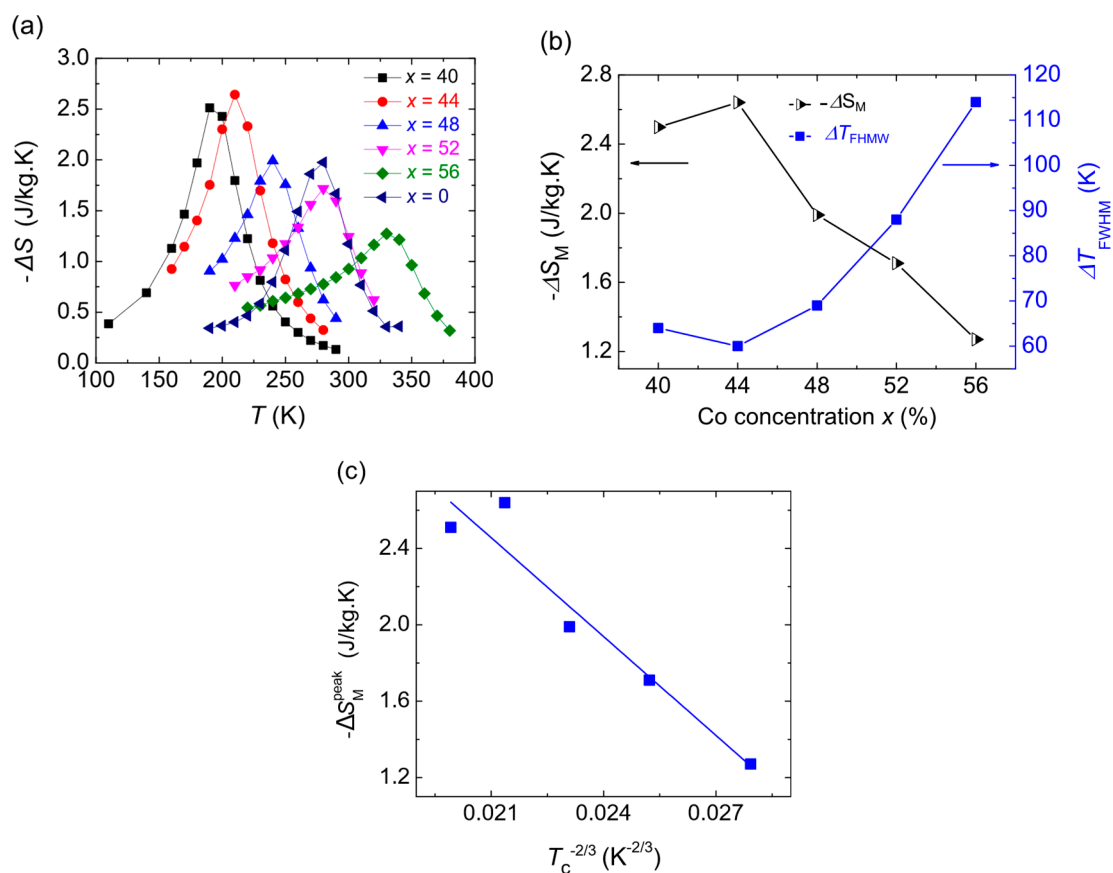


Figure 3. (a) Temperature dependence of the magnetic entropy change, (b) co-concentration dependence of the magnetic entropy change peak and the full width at half maximum (FWHM) of ΔS_m (T) peak, and (c) the dependence of $-\Delta S_M^{\text{peak}}$ as a function of $T_c^{-2/3}$ for the studied $Gd_{100-x}Co_x$ alloys compounds under an applied magnetic field of $\Delta H = 20$ kOe.

In addition to the isothermal entropy change, the relative cooling power (RCP) is also a key parameter to evaluate the magnetocaloric performance. The RCP considers both the isothermal magnetic entropy change and the working temperature range of magnetocaloric materials, and it is given by the following formula:

$$RCP = -\Delta S_M \times \delta T_{FWHM}$$

where T_{FWHM} is the full width at half maximum obtained from the temperature at half the maximum peak value of the ΔS_M curve. Figure 4 shows the evolution of the RCP of the $Gd_{100-x}Co_x$ thin films as a function of the applied magnetic field. The RCP value increases with the applied magnetic field.

Moreover, all the studied $\text{Gd}_{100-x}\text{Co}_x$ alloys present a large RCP value around 140 J/kg for $\Delta H = 20 \text{ kOe}$, which is significantly higher than the RCP of the Gd thin films. Table 1 shows a summary of the present results, the MCE properties of the GdCo thin films, as well as some others reported in the literature. The high values of the RCP and $-\Delta S_m$ (T) obtained for the $\text{Gd}_{100-x}\text{Co}_x$ thin film alloys is very promising for magnetic refrigeration applications with a wide temperature range.

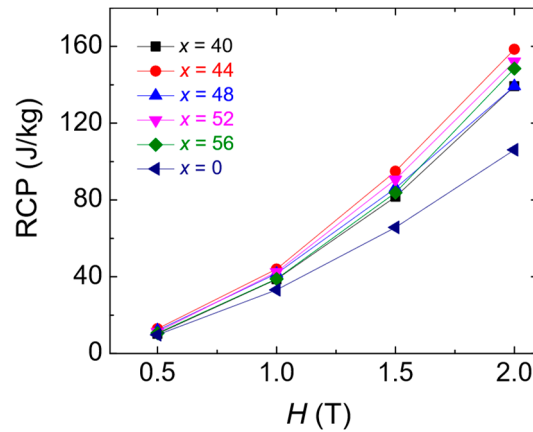


Figure 4. Relative cooling power (RCP) as a function of the applied magnetic field for the $\text{Gd}_{100-x}\text{Co}_x$ alloy films.

Table 1. Magnetic and magnetocaloric properties of $\text{Gd}_{100-x}\text{Co}_x$ compounds with variation in Co doping.

Materials	T_c (K)	$-\Delta S_M^{peak}$ (J/kg.K) $\Delta H = 20 \text{ kOe}$	RCP (J/kg) $\Delta H = 20 \text{ kOe}$	ΔH (T)	References
$\text{Gd}_{60}\text{Co}_{40}$	190	2.51	139	2	This work
$\text{Gd}_{56}\text{Co}_{44}$	205	2.64	158	2	This work
$\text{Gd}_{52}\text{Co}_{48}$	239	1.99	139	2	This work
$\text{Gd}_{48}\text{Co}_{52}$	282	1.71	152	2	This work
$\text{Gd}_{44}\text{Co}_{56}$	337	1.27	148	2	This work
Gd_{100}	280	1.97	106	2	This work
$\text{Gd}_{71}\text{Co}_{29}$ amorphous ribbons	166	3.1	92.3	1	[29]
$\text{Gd}_{62}\text{Co}_{38}$ amorphous ribbons	193	2.8	81.4	1	[29]

3.3. Universal Scaling Analysis

Universal scaling analysis indicates that the Co helps to homogenize the magnetic properties in GdCo thin films [25]. Such a method should remove the temperature and field dependence of the set of $\Delta S(\Delta H, T)$ curve (for fixed ΔH), so that all curves processed with the same scaling protocol collapse onto a single universal curve. A failure to display this universal collapse can be attributed to material inhomogeneity [30], likely in the form of a distribution of exchange energies. Figure 5 shows the universal curve construction for each of the studied $\text{Gd}_{100-x}\text{Co}_x$ thin films by plotting $\Delta S'$ against θ , where $\Delta S' = \Delta S_M / \Delta S_M^{peak}$ is the rescaled entropy change and θ is the rescaled temperature variable as follows:

$$\theta = \begin{cases} -(T - T_c) / (T_{r1} - T_c) & T \leq T_c \\ (T - T_c) / (T_{r2} - T_c) & T \geq T_c \end{cases}$$

with T_{r1} and T_{r2} are reference temperatures chosen at 50% of ΔS_{max} above T_c . As shown in Figure 5, the curves do not collapse into one single curve. Moreover, one can see from Figure 5 that the degree

of collapse increases with the Co concentration. It has been shown that a failure to collapse (such as seen for $x = 44$) can be attributed to inhomogeneity within the material.

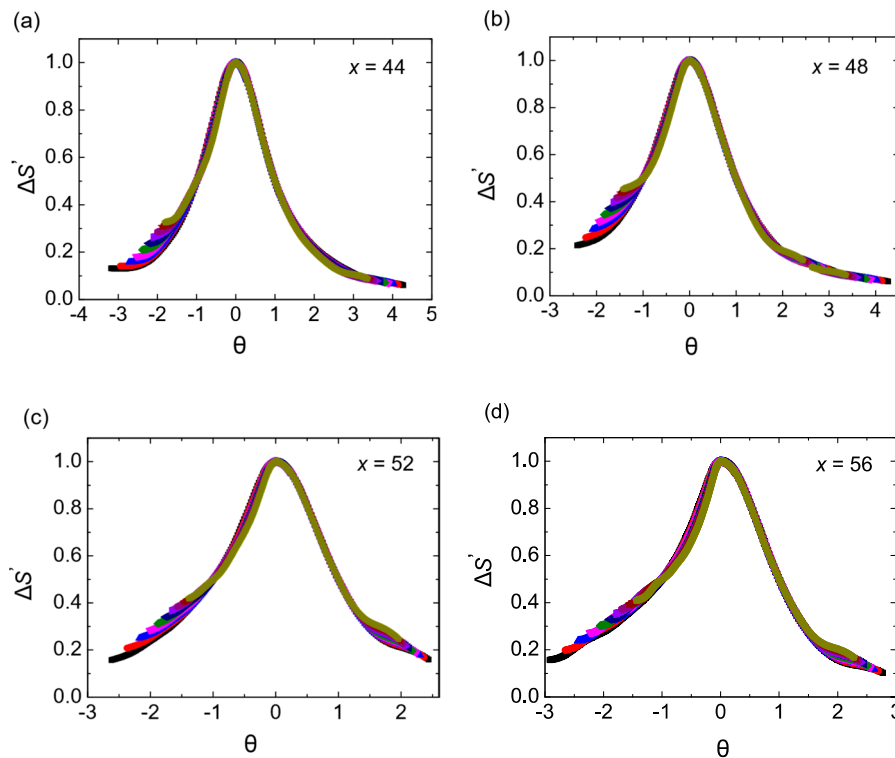


Figure 5. The normalized entropy changes as a function of the rescaled temperature θ for different applied fields for $\text{Gd}_{100-x}\text{Co}_x$ (a) $x = 44$, (b) $x = 48$, (c) $x = 52$, and (d) $x = 56$ thin films.

3.4. Critical Exponents

The second-order ferromagnetic to paramagnetic transition near the Curie temperature can be characterized by a set of critical exponents, where β corresponds to the spontaneous magnetization, γ corresponds to the initial susceptibility, and δ corresponds to the critical magnetization isotherm at T_c . The critical exponents possess the following power-law dependences [31]:

$$M_s(0, T) = m_0 |\varepsilon|^\beta, \varepsilon \leq 0 \quad (1)$$

$$\chi_0^{-1}(0, T) = \frac{h_0}{m_0} |\varepsilon|^\gamma, \varepsilon \geq 0 \quad (2)$$

where $\varepsilon = (T - T_c)/T_c$ is the reduced temperature, and m_0 and $\frac{h_0}{m_0}$ are the critical amplitudes. Initial values of $\beta = 0.4$ and $\gamma = 1.33$ are selected, then a plot of $M^{1/\beta}$ as a function of $(H/M)^{1/\gamma}$ was obtained [12]. The high field linear region ($H > 1$) is used for the analysis, because the Modified Arrott Plots (MAPs) tend to deviate from linearity at low field due to the mutually misaligned magnetic domains. The values of M_s and χ_0^{-1} can be then determined from the intersection of the linearly extrapolated curves with the $M^{1/\beta}$ and $(H/M)^{1/\gamma}$, respectively. Figure 6a shows the temperature dependence of $\chi_0^{-1}(T)$ and $M_s(T)$, which are fitted with Equations (1) and (2). The fitting enables us to obtain new values of β and γ , which are then used to construct new MAPs. These steps are therefore repeated until the iterations converge to the optimum values of β , γ , and T_c . Therefore, the MAPs shown in Figure 6a yielded the following results: $\beta = 0.47 \pm 0.009$ and $\gamma = 1.15 \pm 0.1$. Figure 6b depicts the modified Arrott plots, which show that all lines are parallel to each other. On the other hand, the

fitting of the M - H measured at T close to T_c using Equation (3) enables to extract the value of the critical component δ :

$$H = DM^\delta, t = 0 \tag{3}$$

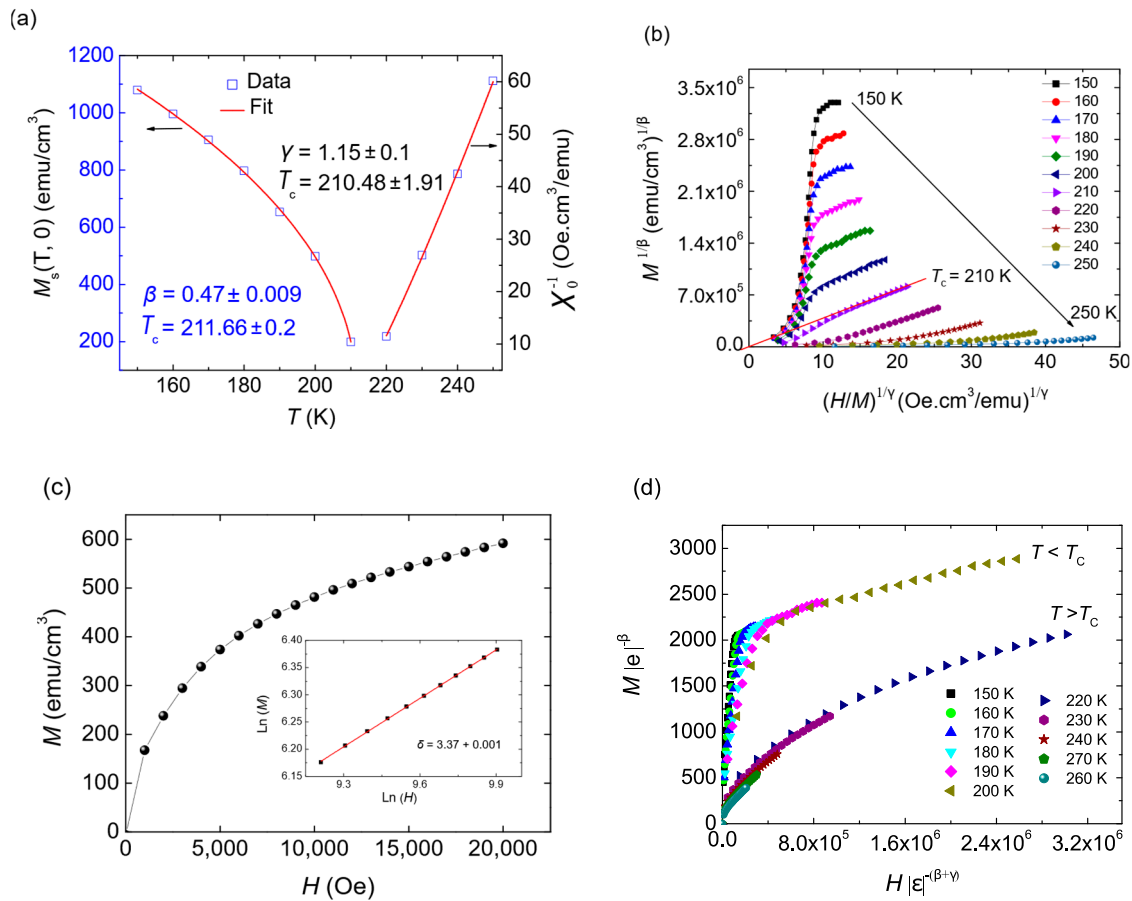


Figure 6. (a) Spontaneous magnetization and inverse of initial susceptibility vs. temperature, (b) modified Arrott plot isotherms of $M^{1/\beta} \sim (H/M)^{1/\gamma}$ with the calculated exponents, (c) isothermal $M(H)$ plots with the log–log scale at $T_c = 210$ K, and (d) scaling plot with $M(H, \varepsilon)\varepsilon^{-\beta}$ versus $H\varepsilon^{-(\beta+\gamma)}$ below and above T_c using exponent determined from the modified Arrott plot of $Gd_{56}Co_{44}$ alloy film.

Figure 6c shows the magnetic field dependence of magnetization at T_c for $Gd_{56}Co_{44}$ alloy film, while the critical isotherm on a log–log scale is shown in the inset. The extracted value of δ is 3.37 ± 0.001 . δ can also be extracted via the Widom scaling relation [32]:

$$\delta = 1 + \frac{\gamma}{\beta}$$

By using the critical parameters β and γ obtained via the MAPs, we deduce from the Widom scaling relation a δ value of 3.44, thus confirming the reliability of the critical exponents extracted from the experimental data. Moreover, the reliability of β and γ can be confirmed via the following scaling hypothesis:

$$M(H, \varepsilon) = \varepsilon^\beta f_\pm(H/\varepsilon^{\beta+\gamma})$$

where f_\pm are regular analytical functions with f_+ and f_- for above and below T_c , respectively. The scaling relation indicates that $M(H, \varepsilon)\varepsilon^{-\beta}$ as a function $H\varepsilon^{-(\beta+\gamma)}$ should yield two universally different branches, one for $T > T_c$ and the other for $T < T_c$. By using the values of β , γ , and T_c from the MAPs method in Figure 6d, one can clearly see that magnetization data falls into two universal curves, one

for $T > T_c$ and the other for $T < T_c$, which agrees with the scaling theory and confirms that the obtained values for the critical exponents and T_c are reliable. Moreover, these critical exponents are very similar to the theoretical values from the mean field model ($\gamma = 1.0$, $\beta = 0.5$, and $\delta = 3$) [33]. We also analyzed the critical behavior of magnetic phase transition using Arrott plots for $\text{Gd}_{100-x}\text{Co}_x$ ($x = 40, 48, 52$, and 56), which follows the mean field model. Consistent with the existence of long-range ferromagnetic interaction, the critical behavior analysis in the vicinity of T_c demonstrates that the magnetism of the GdCo thin films is governed by the long range nature of ferrimagnetism in this system.

4. Conclusions

In summary, we fabricated $\text{Gd}_{100-x}\text{Co}_x$ alloy films on a silicon substrate using sputtering techniques. The magnetic and magnetocaloric effect of $\text{Gd}_{100-x}\text{Co}_x$ ($x = 44, 48, 52, 56$) thin films were investigated. The Curie temperature increases with the Co concentration, and the maximal magnetic entropy change reaches a maximum at the Curie temperature. Under an applied magnetic field of $\Delta H = 20$ kOe, the value of $-\Delta S_M$ is found to be 2.64 for $x = 44$. Moreover, the studied $\text{Gd}_{100-x}\text{Co}_x$ alloy films present an important relative cooling power (RCP) higher than 140 J/kg. Moreover, the investigation of the critical properties of the second-order ferromagnetic transition of the $\text{Gd}_{100-x}\text{Co}_x$ alloy films demonstrate that the magnetic interaction around T_c can be described with the mean field model corresponding to long-range interaction.

Supplementary Materials: The following are available online at <http://www.mdpi.com/2073-4352/9/6/278/s1>.

Author Contributions: Conceptualization, S.M., C.-H.L., M.S.E.H., O.M. and A.B.; methodology, C.-H.L. and M.T.; formal analysis, M.T. and C.-H.L.; investigation, M.T. and C.-H.L.; writing—original draft preparation, M.T. and O.M.; writing—review and editing, M.S.E.H., M.T. and O.M.; visualization, M.S.E.H. and M.T.; supervision, S.M., O.M., A.B., M.H., and M.B.

Funding: This work was funded by the MESRSFC in the framework of the national program PPR under contract No. PPR/2015/57 and by PHC Toubkal/17/49 project.

Acknowledgments: We would like to thank S. Suire, C.-S. Chang, and T. Hauet for technical assistance with the SQUID-VSM measurements.

Conflicts of Interest: The authors declare no conflict of interest.

References

- Gschneidner, K.A., Jr.; Pecharsky, V.K. Thirty years of near room temperature magnetic cooling: Where we are today and future prospects. *Int. J. Refrig.* **2008**, *31*, 945–961. [CrossRef]
- Fujita, A.; Yako, H. Stability of metallic, magnetic and electronic states in NaZn_{13} -type $\text{La}(\text{Fe}_x\text{Si}_{1-x})_{13}$ magnetocaloric compounds. *Scr. Mater.* **2012**, *67*, 578–583. [CrossRef]
- Liu, E.K.; Wang, W.H.; Lin, F.; Zhu, W.; Li, G.J.; Chen, J.L.; Zhang, H.W.; Wu, G.H.; Jiang, C.B.; Xu, H.B.; et al. Stable magnetostructural coupling with tunable magnetoresponse effects in hexagonal ferromagnets. *Nat. Commun.* **2012**, *3*, 873. [CrossRef] [PubMed]
- Trung, N.T.; Zhang, L.; Caron, L.; Buschow, K.H.J.; Brück, E. Giant magnetocaloric effects by tailoring the phase transitions. *Appl. Phys. Lett.* **2010**, *96*, 172504. [CrossRef]
- Gschneidner, K.A., Jr.; Pecharsky, V.K.; Tsokol, A.O. Recent developments in magnetocaloric materials. *Rep. Prog. Phys.* **2005**, *68*, 1479–1539. [CrossRef]
- Pecharsky, V.K.; Gschneidner, K.A., Jr. Giant Magnetocaloric Effect in $\text{Gd}_5(\text{Si}_2\text{Ge}_2)$. *Phys. Rev. Lett.* **1997**, *78*, 4494. [CrossRef]
- Wada, H.; Tanabe, Y. Giant magnetocaloric effect of $\text{MnAs}_{1-x}\text{Sb}_x$. *Appl. Phys. Lett.* **2001**, *79*, 3302. [CrossRef]
- Hu, F.; Shen, B.; Sun, J.; Cheng, Z.; Rao, G.; Zhang, X. Influence of negative lattice expansion and metamagnetic transition on magnetic entropy change in the compound $\text{LaFe}_{11.4}\text{Si}_{1.6}$. *Appl. Phys. Lett.* **2001**, *78*, 3675. [CrossRef]
- Fujita, A.; Fujieda, S.; Hasegawa, Y.; Fukamichi, K. Itinerant-electron metamagnetic transition and large magnetocaloric effects in $\text{La}(\text{Fe}_x\text{Si}_{1-x})_{13}$ compounds and their hydrides. *Phys. Rev. B* **2003**, *67*, 104416. [CrossRef]

10. Tegus, O.; Brück, E.; Buschow, K.H.J.; de Boer, F.R. Transition-metal-based magnetic refrigerants for room-temperature applications. *Nature* **2002**, *415*, 150–152. [[CrossRef](#)] [[PubMed](#)]
11. Krenke, T.; Duman, E.; Acet, M.; Wassermann, E.F.; Mañosa, L.; Planes, A. Inverse magnetocaloric effect in ferromagnetic Ni–Mn–Sn alloys. *Nat. Mater.* **2005**, *4*, 450–454. [[CrossRef](#)]
12. Miller, C.W.; Williams, D.V.; Bingham, N.S.; Srikanth, H. Magnetocaloric effect in Gd/W thin film heterostructures. *J. Appl. Phys.* **2010**, *107*, 09A903. [[CrossRef](#)]
13. Miller, C.W.; Belyea, D.D.; Kirby, B.J. Magnetocaloric effect in nanoscale thin films and heterostructures. *J. Vac. Sci. Technol.* **2014**, *32*, 040802. [[CrossRef](#)]
14. Zhang, Q.; Thota, S.; Guillou, F.; Padhan, P.; Hardy, V.; Wahl, A.; Prellier, W. Magnetocaloric effect and improved relative cooling power in (La_{0.7}Sr_{0.3}MnO₃/SrRuO₃) superlattices. *J. Phys. Condens. Matter* **2001**, *23*, 052201. [[CrossRef](#)]
15. Oumezzine, M.; Galca, A.-C.; Pasuk, I.; Chirila, C.; Leca, A.; Kuncser, V.; Tanase, L.C.; Kumcser, A.; Ghica, C.; Oumezzine, M. Structural, magnetic and magnetocaloric effects in epitaxial La_{0.67}Ba_{0.33}Ti_{0.02}Mn_{0.98}O₃ ferromagnetic thin films grown on 001-oriented SrTiO₃ substrates. *Dalt. Trans.* **2016**, *45*, 15034–15040. [[CrossRef](#)]
16. Zhou, T.; Cher, M.K.; Shen, L.; Hu, J.F.; Yuan, Z.M. On the origin of giant magnetocaloric effect and thermal hysteresis in multifunctional α -FeRh thin films. *Phys. Lett. A* **2013**, *377*, 3052–3059. [[CrossRef](#)]
17. Recarte, V.; Pérez-Landazábal, J.I.; Sánchez-Alárco, V.; Chernenko, A.; Ohtsuka, M. Magnetocaloric effect linked to the martensitic transformation in sputter-deposited Ni–Mn–Ga thin films. *Appl. Phys. Lett.* **2009**, *95*, 141908. [[CrossRef](#)]
18. Mosca, D.H.; Vidal, F.; Etgens, V.H. Strain engineering of the magnetocaloric effect in MnAs epilayers. *Phys. Rev. Lett.* **2008**, *101*, 125503. [[CrossRef](#)]
19. Franco, V.; Blázquez, J.S.; Ingale, B.; Conde, A. The magnetocaloric effect and magnetic refrigeration near room temperature: Materials and models. *Annu. Rev. Mater. Res.* **2012**, *42*, 305–342. [[CrossRef](#)]
20. Gschneidner, K.A., Jr.; Pecharsky, V.K. Magnetocaloric materials. *Annu. Rev. Mater. Sci.* **2000**, *30*, 387–429. [[CrossRef](#)]
21. Phan, M.H.; Yu, S.C. Review of the magnetocaloric effect in manganite materials. *J. Magn. Magn. Mater.* **2007**, *308*, 325–340. [[CrossRef](#)]
22. Lampen, P.; Bingham, N.S.; Phan, M.H.; Kim, H.; Osofsky, M.; Piqué, A.; Phan, T.L.; Yu, S.C.; Srikanth, H. Impact of reduced dimensionality on the magnetic and magnetocaloric response of La_{0.7}Ca_{0.3}MnO₃. *Appl. Phys. Lett.* **2013**, *102*, 062414. [[CrossRef](#)]
23. Lampen-Kelley, P.J. Low Dimensionality Effects in Complex Magnetic Oxides. Ph.D. Thesis, University of South Florida, Tampa, FL, USA, 2015.
24. Khovaylo, V.V.; Rodionova, V.V.; Shevyrtalov, S.N.; Novosad, V. Magnetocaloric effect in reduced dimensions: Thin films, ribbons, and microwires of Heusler alloys and related compounds. *Phys. Status Solidi B* **2014**, *251*, 2104–2113. [[CrossRef](#)]
25. Tadout, M.; Lambert, C.H.; El Hadri, M.S.; Mounkachi, O.; Benyoussef, A.; Hamedoun, M.; Benaissa, M.; Mangin, S. Engineered Gd-Co based multilayer stack to enhanced magneto-caloric effect and relative cooling power. *J. Appl. Phys.* **2018**, *123*, 053902. [[CrossRef](#)]
26. Hansen, P.; Clausen, C.; Much, G.; Rosenkranz, M.; Witter, K. Magnetic and magneto-optical properties of rare-earth transition-metal alloys containing Gd, Tb, Fe, Co. *J. Appl. Phys.* **1989**, *66*, 756. [[CrossRef](#)]
27. Inoue, J.; Shimizu, M. Volume dependence of the first-order transition temperature for RCo₂ compound. *J. Phys. F Met. Phys.* **1982**, *12*, 1811. [[CrossRef](#)]
28. Banerjee, B.K. On a generalised approach to first and second order magnetic transitions. *Phys. Lett.* **1964**, *12*, 16–17. [[CrossRef](#)]
29. Zhang, C.L.; Wang, D.H.; Han, Z.D.; Xuan, H.C.; Gu, B.X.; Du, Y.W. Large magnetic entropy changes in Gd–Co amorphous ribbons. *J. Appl. Phys.* **2009**, *105*, 013912. [[CrossRef](#)]
30. Franco, V.; Blázquez, J.S.; Conde, A. Field dependence of the magnetocaloric effect in materials with a second order phase transition: A master curve for the magnetic entropy change. *Appl. Phys. Lett.* **2006**, *89*, 222512. [[CrossRef](#)]
31. Franco, V.; Caballero-Flores, R.; Condea, A.; Dong, Q.Y.; Zhang, H.W. The influence of a minority magnetic phase on the field dependence of the magnetocaloric effect. *J. Magn. Magn. Mater.* **2009**, *321*, 1115–1120. [[CrossRef](#)]

32. Widom, B. Equation of state in the neighborhood of the critical point. *J. Chem. Phys.* **1965**, *43*, 3898. [[CrossRef](#)]
33. Sahana, M.; Rössler, U.K.; Ghosh, N.; Elizabeth, S.; Bhat, H.L.; Dörr, K.; Eckert, D.; Wolf, M.; Müller, K.-H. Critical properties of the double-exchange ferromagnet $\text{Nd}_{0.6}\text{Pb}_{0.4}\text{MnO}_3$. *Phys. Rev. B* **2003**, *68*, 144408. [[CrossRef](#)]



© 2019 by the authors. Licensee MDPI, Basel, Switzerland. This article is an open access article distributed under the terms and conditions of the Creative Commons Attribution (CC BY) license (<http://creativecommons.org/licenses/by/4.0/>).